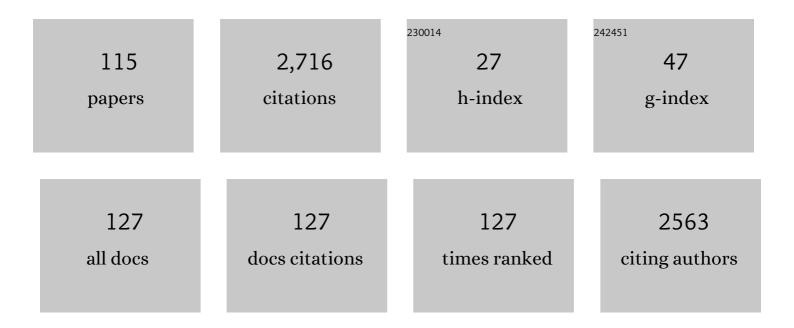


## List of Publications by Year in descending order

Source: https://exaly.com/author-pdf/7455219/publications.pdf Version: 2024-02-01



KAN DALIM

#	Article	IF	CITATIONS
1	Interconnectivity Explains High Canalicular Network Robustness between Neighboring Osteocyte Lacunae in Human Bone. Advanced NanoBiomed Research, 2022, 2, .	1.7	8
2	Clinical Devices for Bone Assessment. Advances in Experimental Medicine and Biology, 2022, 1364, 35-53.	0.8	2
3	Quantitative Ultrasound Assessment of Early Osteoarthritis in Human Articular Cartilage Using a High-Frequency Linear Array Transducer. Ultrasound in Medicine and Biology, 2022, 48, 1429-1440.	0.7	1
4	Estimation of Thickness and Speed of Sound for Transverse Cortical Bone Imaging Using Phase Aberration Correction Methods: An In Silico and Ex Vivo Validation Study. Applied Sciences (Switzerland), 2022, 12, 5283.	1.3	1
5	Estimation of Cortical Bone Microstructure From Ultrasound Backscatter. IEEE Transactions on Ultrasonics, Ferroelectrics, and Frequency Control, 2021, 68, 1081-1095.	1.7	15
6	Bulk Wave Velocities in Cortical Bone Reflect Porosity and Compression Strength. Ultrasound in Medicine and Biology, 2021, 47, 799-808.	0.7	13
7	Pore‣ize Distribution and Frequencyâ€Dependent Attenuation in Human Cortical Tibia Bone Discriminate Fragility Fractures in Postmenopausal Women With Low Bone Mineral Density. JBMR Plus, 2021, 5, e10536.	1.3	11
8	Estimation of Thickness and Speed of Sound in Cortical Bone Using Multifocus Pulse-Echo Ultrasound. IEEE Transactions on Ultrasonics, Ferroelectrics, and Frequency Control, 2020, 67, 568-579.	1.7	25
9	Decreased Compressional Sound Velocity Is an Indicator for Compromised Bone Stiffness in X-Linked Hypophosphatemic Rickets (XLH). Frontiers in Endocrinology, 2020, 11, 355.	1.5	8
10	Anisotropic elastic properties of human cortical bone tissue inferred from inverse homogenization and resonant ultrasound spectroscopy. Materialia, 2020, 11, 100730.	1.3	10
11	Femur strength predictions by nonlinear homogenized voxel finite element models reflect the microarchitecture of the femoral neck. Medical Engineering and Physics, 2020, 79, 60-66.	0.8	12
12	Cortical thinning and accumulation of large cortical pores in the tibia reflect local structural deterioration of the femoral neck. Bone, 2020, 137, 115446.	1.4	9
13	High frequency ultrasound assesses transient changes in cartilage under osmotic loading. Mathematical Biosciences and Engineering, 2020, 17, 5190-5211.	1.0	Ο
14	Acoustic diffusion constant of cortical bone: Numerical simulation study of the effect of pore size and pore density on multiple scattering. Journal of the Acoustical Society of America, 2019, 146, 1015-1023.	0.5	12
15	Large cortical bone pores in the tibia are associated with proximal femur strength. PLoS ONE, 2019, 14, e0215405.	1.1	18
16	Ex vivo cortical porosity and thickness predictions at the tibia using full-spectrum ultrasonic guided-wave analysis. Archives of Osteoporosis, 2019, 14, 21.	1.0	24
17	In Vivo Measurements of Cortical Thickness and Porosity at the Proximal Third of the Tibia Using Guided Waves: Comparison with Site-Matched Peripheral Quantitative Computed Tomography and Distal High-Resolution Peripheral Quantitative Computed Tomography. Ultrasound in Medicine and Biology, 2019, 45, 1234-1242.	0.7	39
18	Functional regulation of YAP mechanosensitive transcriptional coactivator by Focused Low-Intensity Pulsed Ultrasound (FLIPUS) enhances proliferation of murine mesenchymal precursors. PLoS ONE, 2018, 13, e0206041.	1.1	17

#	Article	IF	CITATIONS
19	BMD-based assessment of local porosity in human femoral cortical bone. Bone, 2018, 114, 50-61.	1.4	17
20	Transplantation of Chemically Processed Decellularized Meniscal Allografts. Cartilage, 2017, 8, 180-190.	1.4	11
21	Ultrasound palpation for fast in-situ quantification of articular cartilage stiffness, thickness and relaxation capacity. Biomechanics and Modeling in Mechanobiology, 2017, 16, 1171-1185.	1.4	5
22	Regular chondrocyte spacing is a potential cause for coherent ultrasound backscatter in human articular cartilage. Journal of the Acoustical Society of America, 2017, 141, 3105-3116.	0.5	7
23	Numerical evaluation of the backward propagating acoustic field in healing long bones. Journal of the Acoustical Society of America, 2017, 142, 962-973.	0.5	3
24	Notice of Removal: Assessment of cortical bone pore dimensions by high-frequency backscatter. , 2017, , .		0
25	Notice of Removal: Measurement of ultrasound attenuation, phase velocity and scattering mean free path in cortical bone using independent scattering approximation. , 2017, , .		0
26	Imaging of cortical pores using ultrasound contrast agents: Phantom and ex vivo studies. , 2017, , .		0
27	Imaging of cortical pores using ultrasound contrast agents: An ex-vivo study. , 2017, , .		0
28	Computational Study of the Effect of Cortical Porosity on Ultrasound Wave Propagation in Healthy and Osteoporotic Long Bones. Materials, 2016, 9, 205.	1.3	4
29	Activation of Mechanosensitive Transcription Factors in Murine C2C12 Mesenchymal Precursors by Focused Low-Intensity Pulsed Ultrasound (FLIPUS). IEEE Transactions on Ultrasonics, Ferroelectrics, and Frequency Control, 2016, 63, 1505-1513.	1.7	10
30	Can a continuous mineral foam explain the stiffening of aged bone tissue? A micromechanical approach to mineral fusion in musculoskeletal tissues. Bioinspiration and Biomimetics, 2016, 11, 035004.	1.5	18
31	Species-Independent Modeling of High-Frequency Ultrasound Backscatter in Hyaline Cartilage. Ultrasound in Medicine and Biology, 2016, 42, 1375-1384.	0.7	5
32	Influence of Donor Age and Stimulation Intensity on Osteogenic Differentiation of Rat Mesenchymal Stromal Cells in Response to Focused Low-Intensity Pulsed Ultrasound. Ultrasound in Medicine and Biology, 2016, 42, 2965-2974.	0.7	7
33	Multimodal correlative investigation of the interplaying micro-architecture, chemical composition and mechanical properties of human cortical bone tissue reveals predominant role of fibrillar organization in determining microelastic tissue properties. Acta Biomaterialia, 2016, 44, 51-64.	4.1	20
34	Full-Field Calcium K-Edge X-ray Absorption Near-Edge Structure Spectroscopy on Cortical Bone at the Micron-Scale: Polarization Effects Reveal Mineral Orientation. Analytical Chemistry, 2016, 88, 3826-3835.	3.2	18
35	A Focused Low-Intensity Pulsed Ultrasound (FLIPUS) System for Cell Stimulation: Physical and Biological Proof of Principle. IEEE Transactions on Ultrasonics, Ferroelectrics, and Frequency Control, 2016, 63, 91-100.	1.7	17
36	Stimulation of Bone Repair with Ultrasound. Advances in Experimental Medicine and Biology, 2016, 880, 385-427.	0.8	27

Кау Каим

#	Article	IF	CITATIONS
37	Elasticity–density and viscoelasticity–density relationships at the tibia mid-diaphysis assessed from resonant ultrasound spectroscopy measurements. Biomechanics and Modeling in Mechanobiology, 2016, 15, 97-109.	1.4	45
38	3D ultrasound biomicroscopy for assessment of cartilage repair tissue: volumetric characterisation and correlation to established classification systems. , 2016, 31, 119-135.		9
39	In-silico evaluation of cortical porosity by tangential axial transmission. , 2015, , .		1
40	Activation of mechanosensitive transcription factors in murine C2C12 myoblasts by focused low-intensity pulsed Ultrasound (FLIPUS). , 2015, , .		1
41	Mechanosensitive response of murine C2C12 myoblasts to focused Low-Intensity Pulsed Ultrasound (FLIPUS) stimulation. , 2015, , .		2
42	Distribution of mesoscale elastic properties and mass density in the human femoral shaft. Connective Tissue Research, 2015, 56, 120-132.	1.1	11
43	Ultrasound propagation in cortical bone: Axial transmission and backscattering simulations. , 2015, 2015, 1456-9.		1
44	High-frequency cortical backscatter reveals cortical microstructure - A simulation study. , 2015, , .		5
45	Prospective discrimination of vertebral fractures by axial transmission ultrasound using optimized first arriving signal velocity measurements. , 2015, , .		2
46	Numerical simulation of high-frequency ultrasound scattering on articular cartilage cellular structure. , 2015, , .		0
47	The effect of cortical bone porosity on ultrasonic backscattering parameters. , 2015, , .		4
48	Multisite ultrasound axial transmission study in postmenopausal women using optimized first arriving signal velocity measurements. , 2015, , .		2
49	Canalicular Network Morphology Is the Major Determinant of the Spatial Distribution of Mass Density in Human Bone Tissue: Evidence by Means of Synchrotron Radiation Phase-Contrast nano-CT. Journal of Bone and Mineral Research, 2015, 30, 346-356.	3.1	108
50	Skeletal maturation substantially affects elastic tissue properties in the endosteal and periosteal regions of loaded mice tibiae. Acta Biomaterialia, 2015, 21, 154-164.	4.1	9
51	Synchrotron X-ray phase nano-tomography-based analysis of the lacunar–canalicular network morphology and its relation to the strains experienced by osteocytes in situ as predicted by case-specific finite element analysis. Biomechanics and Modeling in Mechanobiology, 2015, 14, 267-282.	1.4	83
52	Impact of chemical composition on microscale elastic properties of cortical bone - A site-matched FTIR-SAM study. , 2015, , .		0
53	Three-dimensional investigation of the relationship between orientation and microelastic properties of mineralized collagen fibrils in human osteonal bone. , 2015, , .		0
54	Low-Intensity Pulsed Ultrasound Improves the Functional Properties of Cardiac Mesoangioblasts. Stem Cell Reviews and Reports, 2015, 11, 852-865.	5.6	21

#	Article	IF	CITATIONS
55	An introduction to measurements of human cortical bone elasticity using Resonant Ultrasound Spectroscopy. , 2015, , .		Ο
56	To what extent can cortical bone millimeter-scale elasticity be predicted by a two-phase composite model with variable porosity?. Acta Biomaterialia, 2015, 12, 207-215.	4.1	20
57	In-vitro stimulation of cells of the musculoskeletal system with focused Low-Intensity Pulsed Ultrasound (FLIPUS): Analyses of cellular activities in response to the optimized acoustic dose. , 2014, ,		3
58	Impact of microscale properties measured by 50-MHz acoustic microscopy on mesoscale elastic and ultimate mechanical cortical bone properties. , 2014, , .		5
59	Application of an effective medium theory for modeling ultrasound wave propagation in healing long bones. Ultrasonics, 2014, 54, 1219-1230.	2.1	26
60	On the elastic properties of mineralized turkey leg tendon tissue: multiscale model and experiment. Biomechanics and Modeling in Mechanobiology, 2014, 13, 1003-1023.	1.4	27
61	Ultrasound biomicroscopy (UBM) and scanning acoustic microscopy (SAM) for the assessment of hernia mesh integration: a comparison to standard histology in an experimental model. Hernia: the Journal of Hernias and Abdominal Wall Surgery, 2014, 18, 579-585.	0.9	9
62	Stimulation of bone repair with ultrasound: A review of the possible mechanic effects. Ultrasonics, 2014, 54, 1125-1145.	2.1	173
63	Accessing osteocyte lacunar geometrical properties in human jaw bone on the submicron length scale using synchrotron radiation 14CT. Journal of Microscopy, 2014, 255, 158-168.	0.8	22
64	Ultrasound to Assess Bone Quality. Current Osteoporosis Reports, 2014, 12, 154-162.	1.5	68
65	Articular cartilage degeneration classification by means of high-frequency ultrasound. Osteoarthritis and Cartilage, 2014, 22, 1577-1582.	0.6	18
66	3D Raman mapping of the collagen fibril orientation in human osteonal lamellae. Journal of Structural Biology, 2014, 187, 266-275.	1.3	80
67	3-D High-Frequency Ultrasound Backscatter Analysis of Human Articular Cartilage. Ultrasound in Medicine and Biology, 2014, 40, 244-257.	0.7	16
68	Modeling of Femoral Neck Cortical Bone for the Numerical Simulation of Ultrasound Propagation. Ultrasound in Medicine and Biology, 2014, 40, 1015-1026.	0.7	19
69	Influence of porosity, pore size, and cortical thickness on the propagation of ultrasonic waves guided through the femoral neck cortex: a simulation study. IEEE Transactions on Ultrasonics, Ferroelectrics, and Frequency Control, 2014, 61, 302-313.	1.7	24
70	Priors for X-ray in-line phase tomography of heterogeneous objects. Philosophical Transactions Series A, Mathematical, Physical, and Engineering Sciences, 2014, 372, 20130129.	1.6	22
71	Multiscale, Converging Defects of Macro-Porosity, Microstructure and Matrix Mineralization Impact Long Bone Fragility in NF1. PLoS ONE, 2014, 9, e86115.	1.1	29
72	Alterations of Mass Density and 3D Osteocyte Lacunar Properties in Bisphosphonate-Related Osteonecrotic Human Jaw Bone, a Synchrotron ÂμCT Study. PLoS ONE, 2014, 9, e88481.	1.1	47

Кау Каим

#	Article	IF	CITATIONS
73	Investigation of the three-dimensional orientation of mineralized collagen fibrils in human lamellar bone using synchrotron X-ray phase nano-tomography. Acta Biomaterialia, 2013, 9, 8118-8127.	4.1	95
74	3-D High-Frequency Ultrasound Improves the Estimation of Surface Properties in Degenerated Cartilage. Ultrasound in Medicine and Biology, 2013, 39, 834-844.	0.7	15
75	The Early Phases of Bone Healing Can Be Differentiated in a Rat Osteotomy Model by Focused Transverse-Transmission Ultrasound. Ultrasound in Medicine and Biology, 2013, 39, 1642-1653.	0.7	14
76	Longitudinal elastic properties and porosity of cortical bone tissue vary with age in human proximal femur. Bone, 2013, 53, 451-458.	1.4	78
77	High-frequency backscatter analysis of human articular cartilage. , 2013, , .		1
78	Microfibril Orientation Dominates the Microelastic Properties of Human Bone Tissue at the Lamellar Length Scale. PLoS ONE, 2013, 8, e58043.	1.1	56
79	Two-dimensional simulations of wave propagation in healing long bones based on scanning acoustic microscopy images. , 2012, , .		2
80	Histogram Feature–Based Classification Improves Differentiability of Early Bone Healing Stages From Micro-Computed Tomographic Data. Journal of Computer Assisted Tomography, 2012, 36, 469-476.	0.5	3
81	Propagation based X-ray phase microtomography of multi-material objects for simultaneous bone and soft tissue visualisation. , 2012, , .		Ο
82	Prediction of the intramuscular fat content in loin muscle of pig carcasses by quantitative time-resolved ultrasound. Meat Science, 2012, 90, 216-225.	2.7	16
83	Spatial distribution of tissue level properties in a human femoral cortical bone. Journal of Biomechanics, 2012, 45, 2264-2270.	0.9	42
84	Ultrasound velocity and attenuation of porcine soft tissues with respect to structure and composition: I. Muscle. Meat Science, 2011, 88, 51-58.	2.7	29
85	Ultrasound velocity and attenuation of porcine soft tissues with respect to structure and composition: II. Skin and backfat. Meat Science, 2011, 88, 67-74.	2.7	25
86	A determination of the minimum sizes of representative volume elements for the prediction of cortical bone elastic properties. Biomechanics and Modeling in Mechanobiology, 2011, 10, 925-937.	1.4	57
87	Spatial-Temporal Mapping of Bone Structural and Elastic Properties in a Sheep Model Following Osteotomy. Ultrasound in Medicine and Biology, 2011, 37, 474-483.	0.7	43
88	Microscopic Elastic Properties. , 2011, , 409-439.		4
89	Multiscale structure-functional modeling of lamellar bone. Proceedings of Meetings on Acoustics, 2010, , .	0.3	2
90	Adaptive Remodeling of Trabecular Bone Core Cultured in 3-D Bioreactor Providing Cyclic Loading: An Acoustic Microscopy Study. Ultrasound in Medicine and Biology, 2010, 36, 999-1007.	0.7	10

#	Article	IF	CITATIONS
91	Quantitative ultrasound biomicroscopy for the analysis of healthy and repair cartilage tissue. , 2010, 19, 58-71.		38
92	Cortical Bone Microelasticity Assessed with Scanning Acoustic Microscopy: Relationship to Nanostructural Characteristics across a Human Osteon. IFMBE Proceedings, 2010, , 190-192.	0.2	0
93	Defective Peripheral Nerve Development Is Linked to Abnormal Architecture and Metabolic Activity of Adipose Tissue in Nscl-2 Mutant Mice. PLoS ONE, 2009, 4, e5516.	1.1	18
94	Signal analysis for the estimation of mechanical parameters of viable cells using GHz-acoustic microscopy. , 2009, , .		1
95	Assessment of Microelastic Properties of Bone Using Scanning Acoustic Microscopy: A Face-to-Face Comparison with Nanoindentation. Japanese Journal of Applied Physics, 2009, 48, 07GK01.	0.8	36
96	Acoustic impedance changes in cartilage and subchondral bone due to primary arthrosis. Ultrasonics, 2008, 48, 613-620.	2.1	28
97	Spatial distribution of anisotropic acoustic impedance assessed by time-resolved 50-MHz scanning acoustic microscopy and its relation to porosity in human cortical bone. Bone, 2008, 43, 187-194.	1.4	32
98	Microelastic imaging of bone. IEEE Transactions on Ultrasonics, Ferroelectrics, and Frequency Control, 2008, 55, 1417-1431.	1.7	73
99	Derivation of the mesoscopic elasticity tensor of cortical bone from quantitative impedance images at the micron scale. Computer Methods in Biomechanics and Biomedical Engineering, 2008, 11, 147-157.	0.9	22
100	Upper limb muscle forces: A comparative study. Computer Methods in Biomechanics and Biomedical Engineering, 2008, 11, 147-148.	0.9	6
101	Scanning acoustic microscopy an application for evaulating varnish layer conditions non-destructively. , 2008, , .		2
102	P5A-9 Depth Dependent High Frequency Backscatter Analysis of Degenerated Cartilage. , 2007, , .		1
103	9D-6 Signal Analysis in Scanning Acoustic Microscopy for Non-Destructive Assessment of Connective Defects in Flip-Chip BGA Devices. Proceedings IEEE Ultrasonics Symposium, 2007, , .	0.0	3
104	Variations of microstructure, mineral density and tissue elasticity in B6/C3H mice. Bone, 2007, 41, 1017-1024.	1.4	36
105	Assessment of Anisotropic Tissue Elasticity of Cortical Bone from High-Resolution, Angular Acoustic Measurements. IEEE Transactions on Ultrasonics, Ferroelectrics, and Frequency Control, 2007, 54, 1560-1570.	1.7	48
106	Preservation of microelastic properties of dentin and tooth enamel in vitro—A scanning acoustic microscopy study. Dental Materials, 2007, 23, 1221-1228.	1.6	42
107	Assessment of composition and anisotropic elastic properties of secondary osteon lamellae. Journal of Biomechanics, 2006, 39, 2282-2294.	0.9	106
108	Prediction of biomechanical stability after callus distraction by high resolution scanning acoustic microscopy. Ultrasound in Medicine and Biology, 2006, 32, 1913-1921.	0.7	17

#	Article	IF	CITATIONS
109	Assessment of bone structure and acoustic impedance in C3H and BL6 mice using high resolution scanning acoustic microscopy. Ultrasonics, 2006, 44, e1307-e1311.	2.1	12
110	Site-matched assessment of structural and tissue properties of cortical bone using scanning acoustic microscopy and synchrotron radiation μCT. Physics in Medicine and Biology, 2006, 51, 733-746.	1.6	75
111	Derivation of elastic stiffness from site-matched mineral density and acoustic impedance maps. Physics in Medicine and Biology, 2006, 51, 747-758.	1.6	95
112	Computation of cortical bone macroscopic properties from microscopic elastic data. , 2006, , 591-591.		0
113	Bone microstructure and elastic tissue properties are reflected in QUS axial transmission measurements. Ultrasound in Medicine and Biology, 2005, 31, 1225-1235.	0.7	121
114	Frequency and resolution dependence of the anisotropic impedance estimation in cortical bone using time-resolved scanning acoustic microscopy. Journal of Biomedical Materials Research - Part A, 2004, 71A, 430-438.	2.1	55
115	Channel defect detection in food packages using integrated backscatter ultrasound imaging. IEEE Transactions on Ultrasonics, Ferroelectrics, and Frequency Control, 1998, 45, 30-40.	1.7	42